Analytical Methods

Accepted Manuscript

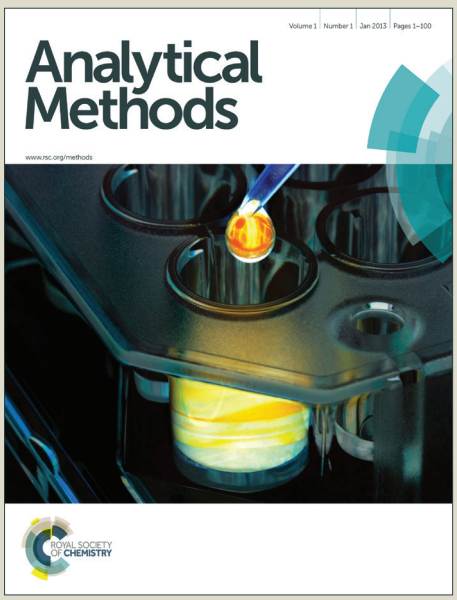

ROYAL SOCIETY OF CHEMISTRY

www.rsc.org/methods

Journal Name

RSCPublishing

ARTICLE

A non-aggregation colorimetric method for trace lead(II) ions based on the leaching of gold nanorods

Cite this: DOI: 10.1039/x0xx00000x

Yu-Ching Lan, and Yang-Wei Lin*

Received 00th January 2012,
Accepted 00th January 2012

DOI: 10.1039/x0xx00000x

www.rsc.org/

We report a simple and fast colorimetric method using gold nanorods (Au NRs) as sensing probes to detect Pb^{2+} ions in complex real samples. The method is based on Pb^{2+} ions increasing the leaching rate of Au NRs induced by thiosulfate ($S_2O_3^{2-}$). A positively charged bilayer of the surfactant cetyltrimethylammonium bromide on the Au NR surfaces facilitates the electrostatic adsorption of $S_2O_3^{2-}$, and the longitudinal surface plasmon resonance absorption of $S_2O_3^{2-}$/Au NRs that are produced is slightly decreased. The formation of Pb–Au alloys on the surfaces of Au NRs leads to a significant decrease in the electrode potential of gold; thus, increasing the dissolution rate of the gold, which is dependent on the Pb^{2+} ion concentration. Using matrix-assisted laser desorption/ionization mass spectrometry, energy-dispersive X-ray spectroscopy, and X-ray photoelectron spectroscopy, we proved that Pb–Au alloys were formed on the Au NR surfaces in the presence of Pb^{2+} ions and $S_2O_3^{2-}$. The reaction temperature and time, the buffer pH, and the $S_2O_3^{2-}$ concentration are important parameters in determining the sensitivity and selectivity of the method for sensing Pb^{2+} ions. Under the optimum conditions (3.0 mM $S_2O_3^{2-}$, 51 pM Au NRs, 10 mM Tris-HCl buffer, pH 8.0), the limit of detection for Pb^{2+} ions, giving a signal-to-noise ratio of 3, was 4.3 nM. We used this nanosensor system to determine Pb^{2+} ions in complex real samples (lake, pond, seawater, urine, and soil samples), and found that this approach offers advantages in terms of its simplicity, accuracy, and precision (the relative standard deviations of triplicate analyses of each sample were below 3%).

Introduction

The important roles of lead (Pb) in biological and environmental systems as well as in chemistry have attracted much attention.[1, 2] Exposure to Pb has been associated with behavioral abnormalities and impairments in learning, hearing, and cognitive functions in humans and experimental animals.[3] The U.S. Environmental Protection Agency (US EPA) has defined the concentration above which Pb causes 75 nM toxicity. Pb can inhibit brain development in children, and the U.S. Food and Drug Administration has suggested that a Pb concentration of 2.5 μM (518 μg L^{-1}) should be used as an "action level" for products intended for children.[4] Inductively coupled plasma mass spectrometry, X-ray fluorescence spectrometry, and anodic stripping voltammetry are powerful techniques for determining metal ion concentrations, but being expensive they not suitable for on-site analysis. It is, therefore, important to develop sensitive, selective, and reliable analytical techniques for determining Pb.

The study of metal particles with well-defined nanostructures has become one of the most active research areas in recent decades.[5-7] Gold nanoparticles (Au NPs) have received considerable attention for use in fields such as chemical and biological sensing, medical diagnostics, therapeutics, and biological imaging.[8-11] Surface plasmon resonance (SPR) absorbance by Au NPs, the extinction coefficients of which can reach as high as 10^{10} M^{-1} cm^{-1}, is extremely sensitive to the nature, sizes, and shapes of the Au NPs, the interparticle distances, and the nature of the surrounding medium.[12] Many colorimetric methods for measuring Pb^{2+} concentrations using DNA-functionalized Au NPs have been reported.[13-15] For example, Lu and coworkers developed a series of functional DNAzyme-based sensors that used Au NPs,[16] and these sensors could be used to detect analytes at concentrations between 3 nM–1 μM. Dong and coworkers developed a DNAzyme-based colorimetric sensor for determining Pb^{2+} that had a limit of detection (LOD) of 500 nM.[17] However, synthesizing DNA oligomers and chemically

modifying them with Au NPs is complex and expensive. Small molecules, proteins, and polymers have also been used to modify Au NPs for detecting Pb^{2+}. For example, Thomas and coworkers used Au NPs functionalized with gallic acid to determine Pb^{2+} and achieved a high level of sensitivity.[18] Wang and coworkers further developed this method to achieve a lower LOD by adding Pb^{2+} when synthesizing the Au NPs to form a Pb–gallic acid complex, which caused the Au NPs to aggregate when they interacted with Pb^{2+}.[19] This method permitted the colorimetric detection of trace Pb^{2+} concentrations with an LOD as low as 25 nM. 11-Mercaptoundecanoic acid, glutathione, and thiol alkyl phosphates have also been used to modify Au NPs for their use in detecting Pb^{2+}.[20-27] Many of these systems are restricted by certain conditions, such as thiol end groups that are easily oxidized, a lack of specificity for Pb^{2+}, and matrix interferences (which are inevitable), so complicated pretreatments of samples are required when these methods are used.

The sensing approaches described above are based on the aggregation of Au NPs, but Huang and coworkers have developed a colorimetric Au NP probe for determining Pb^{2+} that the sensing approach is not based on aggregation, and this provided an LOD of 0.5 nM.[28] This system is based on the fact that the presence of Pb^{2+} ions increases the rate at which Au NPs are leached by thiosulfate ($S_2O_3^{2-}$) and 2-mercaptoethanol (2-ME). However, this method was found not to function in highly saline solutions, and it required 2 h to determine the Pb^{2+} concentration, so it is not suitable for use as a rapid assay. To allow the rapid determination of Pb^{2+} using a nitrocellulose membrane modified with Au NPs (Au NPs/NCM), the same research group developed this method further.[29] This method, assisted by microwave irradiation, allowed Pb^{2+} to be analyzed in 10 min, but preparing the Au NPs/NCM required intensive work in the laboratory. Wu and coworkers recently developed a simple colorimetric probe to determine Pb^{2+} in 30 min with an LOD of 40 nM. This probe was based on the leaching of Au NPs that had been modified with cetyltrimethylammonium bromide (CTAB), caused by the presence of $S_2O_3^{2-}$ and Pb^{2+}.[30] This method is simple, cheap, and environmentally friendly, but its sensitivity needs to be improved to make it suitable for determining Pb^{2+} in complex real samples.

Anisotropic gold nanorods (Au NRs) are formed when small Au NP seeds grow selectively in certain directions. Au NRs have two SPR bands, transverse and longitudinal.[31] The transverse SPR (TSPR) and longitudinal SPR (LSPR) bands are extremely sensitive to changes in the aspect ratios (length/width) of the Au NRs and to the dielectric properties of the surroundings,[32, 33] so the potential for using Au NRs in multiplexed biological sensing and biomedical imaging applications has been recognized.[34] The sensitivity of Au NRs to analytes such as metal ions, aminothiols, DNA, and proteins has been demonstrated both theoretically and experimentally.[35-42] Therefore, we attempted to use Au NRs nanoprobes to selectively determine trace Pb^{2+} ions through Pb^{2+} increasing the rate at which the Au NRs are leached by $S_2O_3^{2-}$. In this system, changes in the color and SPR band ratio (LSPR/TSPR) in the solution were dependent on the Pb^{2+} concentration at a constant Au NR concentration. The effects of reaction temperature, reaction time, buffer pH, buffer concentration, and $S_2O_3^{2-}$ concentration on the selectivity and sensitivity of the $S_2O_3^{2-}$/Au NR probe for Pb^{2+} were evaluated. The practicality of using the $S_2O_3^{2-}$/Au NR probe was then validated by determining Pb^{2+} in environmental water (lake, pond, and seawater) samples and in samples of more complicated matrices (urine and soil).

Experimental sections

Chemicals

All of the chemicals used were of analytical grade or of the highest purity that was available. Hydrogen tetrachloroaurate (III) trihydrate ($HAuCl_4 \cdot 3H_2O$), silver nitrate ($AgNO_3$, 99%), L-ascorbic acid (99%), CTAB (98%), sodium borohydride ($NaBH_4$, 98%), $Pb(NO_3)_2$, $Ni(NO_3)_2 \cdot 6H_2O$, $Cr(NO_3)_3 \cdot 9H_2O$, NaCl, $CaCl_2 \cdot 2H_2O$, $Sr(NO_3)_2$, $BaCl_2 \cdot 6H_2O$, $Cd(NO_3)_2 \cdot 4H_2O$, $FeCl_2 \cdot 4H_2O$, $Mg(NO_3)_2 \cdot 6H_2O$, $FeCl_3$, $HgCl_2$, $Co(NO_3)_2 \cdot 6H_2O$, $Cu(NO_3)_2 \cdot 2.5H_2O$, and KCl were obtained from Sigma Aldrich (St. Louis, MO, USA). Tris (base) was purchased from J. T. Baker (Phillipsburg, NJ, USA). The Tris (0.1 M) solutions were adjusted to pH 8.0 using 2.0 M HCl. Deionized water (18.2 MΩ·cm) was used to prepare all of the aqueous solutions.

Preparation of Au NRs

The Au NR seeds were prepared using a slightly modified seeding method that has been described previously.[43] An aqueous 0.2 M CTAB solution (5.0 mL) was mixed with 0.5 mM $HAuCl_4$ (5.0 mL), followed by sonicating the solution while adding ice-cold 0.01 M $NaBH_4$ (0.6 mL). The mixture was allowed to react for 3 min, after which it formed a brownish yellow seed solution. For the growth solution, 0.2 M CTAB (50.0 mL) was mixed with 1.0 mM $HAuCl_4$ (50.0 mL) and 0.1 M $AgNO_3$ (0.1 mL). The mixture was mixed gently, followed by adding 78.8 mM ascorbic acid (0.7 mL) to act as a mild reducing agent. The growth solution rapidly changed from dark yellow to colorless indicating the formation of $AuCl_2^-$ ions. Finally, an aliquot of the seed solution (0.12 mL) was added to the growth solution, and the mixture gradually turned dark pink over a period of 30 min, indicating the formation of Au NRs. Before Pb^{2+} ions sensing, the as-prepared Au NR solutions (100.0 mL) were subjected to one wash-centrifugation cycle to remove excess CTAB; centrifugation was conducted at 12,000 rpm for 10 min and deionized water (10.0 mL) was used for washing in the cycle. The purified Au NR solution (0.51 nM) was used to determine Pb^{2+} ions.[44]

Characterization

The UV–Vis absorption spectra of Au NRs were recorded using a UV–Vis spectrometer (Evolution 200; Thermo Fisher, Waltham, MA, USA). A JEOL-1200EX II (JEOL, Tokyo, Japan) transmission electron microscopy (TEM) system was used to measure the size and shape of the Au NRs. An energy-

dispersive X-ray spectroscopy (EDS) system (Oxford Instruments, Abingdon, UK) was used to confirm the compositions of the gold nanostructures that were prepared. FT-IR and Raman spectra of the Au NRs were collected, at room temperature, using an Agilent Cary 600 Series FT-IR (Agilent Technologies, Santa Clara, CA, USA) and a confocal micro-Raman system (Thermo Fisher, Waltham, MA, USA), respectively. Mass spectra were collected using a Microflex matrix-assisted laser desorption/ionization-time of flight mass spectrometer (MALDI-MS; Bruker Daltonics, Bremen, Germany) in positive ionization mode. X-ray photoelectron spectroscopy (XPS) was performed using a VG ESCA210 electron spectroscopy (VG Scientific, West Sussex, UK). The zeta potentials of the Au NRs were measured using a Zetasizer Nano ZS90 apparatus (Malvern Instruments, Malvern, UK).

General Procedure for Colorimetric Analysis

Most of the metal salts used in this study were nitrates. Stock solutions of the metal ions (0.1 M) were prepared in 0.1 M HNO_3, then diluted to 0–100 μM in ultrapure water. For the selective determinations of Pb^{2+} ions, 50 μL aliquots of metal ion solutions were added to 10 mM Tris-HCl buffer (pH 8.0) solutions containing 51 pM Au NRs, and 3.0 mM $Na_2S_2O_3$, to give final volumes of 500 μL. The mixtures were equilibrated at 50 °C for 10 min, later transferred to 96 well microtiter plates. Later, the absorbance spectra were recorded using a Synergy H1 Hybrid Multi-Mode Microplate Reader (Biotek Instruments, Winooski, VT, USA). The determinations were performed in triplicate.

Pb Determination Procedure for Real Samples Using Atomic Absorption Spectroscopy

Lake and pond water samples as well as soil samples were collected from the campus of the National Changhua University of Education, Taiwan. A seawater sample was collected from the beach in Taichung City. For a urine sample, all ethics statements and consent were written and signed. Experiments were performed in compliance with the relevant laws and institutional guidelines (DOH Regulation No. 0950206912, Taiwan), and were approved by the local research ethics committee (National Changhua University of Education, Taiwan). Informed consent was obtained from a donor. A urine donor was healthy according to World Health Organization standards. For soil sample pre-treatment, each soil sample (1.00 g) was digested in acid following the US EPA Method 305B (USEPA SE-846 in Government Printing Office, Washington, DC, 1996). Soil sample solution was then evaporated to dryness using a SpeedVac concentrator at a medium drying speed. 10 mM Tris-HCl solution (pH 8.0) was then added to the residue, and the concentrated solutions (100×) were mixed using a vortex. Each sample was filtered through a 0.2 μm membrane, and a 100 μL aliquot was spiked with a standard solution of Pb^{2+} at the desired concentration. The spiked sample was then diluted to 500 μL using a solution containing 51 pM Au NRs, 3.0 mM $Na_2S_2O_3$, and 10 mM Tris-HCl buffer at pH 8.0. The spiked samples were analyzed using the method developed and an atomic absorption spectrophotometer (AAS; Sens AA, GBC scientific equipment, Braeside, Australia). The determinations were performed in triplicate.

Results and Discussion

Sensing Approach

The sensing strategy used in this study is illustrated in Scheme 1. $S_2O_3^{2-}$ is known to be an alternative leaching agent for extracting gold. $S_2O_3^{2-}$ was predicted to adsorb onto the Au NR surfaces because of electrostatic interactions between $S_2O_3^{2-}$ and the CTAB on the Au NR surfaces. This will result in a redox reaction occurring at the solid–liquid interface in the presence of oxygen, forming the $Au(S_2O_3)_2^{3-}$ complex and leading to part of the Au NRs dissolving.

$$4Au + O_2 + 2H_2O + 8S_2O_3^{2-} \rightarrow 4Au(S_2O_3)_2^{3-} + 4OH^-$$

However, this reaction is very slow if the gold surface is oxidized because a sulfur-like film can be formed owing to the decomposition of thiosulfate on the gold surface. Adding Pb^{2+} was found to avoid this problem by accelerating the leaching of the Au NRs because of the $AuPb_2$ and $AuPb_3$ alloys formation on the gold surface, leading to a significant decrease in the electrode potential of the gold, and, therefore, an increased dissolution rate.[28] Adding Pb^{2+} to the Au NR solution in the presence of $S_2O_3^{2-}$ led to the Au NRs gradually becoming shorter and the gold nanostructures gradually changing from rods to spheres, and finally becoming completely dissolved. The Au NR solution gradually turned less intensely colored during this process, and this change in color intensity can be used to semi-quantify the amount of Pb^{2+} in the aqueous solution. The SPR band ratio change of the Au NRs can be used to quantify Pb^{2+} in the aqueous solution.

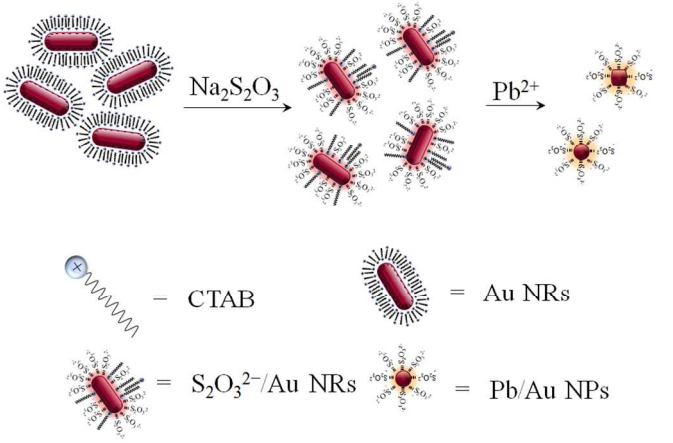

Scheme 1. Schematic representation of the colorimetric method for measuring Pb^{2+} ions, which is based on the Pb^{2+} ions increasing the leaching rate of the Au NRs in the presence of $S_2O_3^{2-}$.

The absorption spectra were monitored, as presented in Figure 1A, to verify the roles that $S_2O_3^{2-}$ and Pb^{2+} played in increasing the leaching rate of the Au NRs, and the TEM

images presented in Figure 1B revealed the corresponding changes in the physical condition of the Au NRs. As observed from curve "a" in Figure 1A, the initial Au NRs exhibited two surface plasmon resonance absorption peaks, at 530 and 750 nm, which corresponded to the TSPR and LSPR bands, respectively. As presented in TEM image "a" in Figure 1B, the initial Au NRs were 36.6 ± 2.7 nm long and 11.4 ± 1.5 nm wide. We demonstrate the Au NRs sample was stable (no precipitates formed) for at least 1 month when stored at room temperature in the dark by TEM and absorption experiments. Furthermore, the TSPR and LSPR bands of the Au NRs for three different batches of Au NRs were reproducible (relative standard deviation less than 2.13%). Both TSPR and LSPR absorption increased when 100 μM Pb^{2+} was added to the solution (Figure 1A curve "b"). A small amount of Pb–Au alloys ($AuPb_2$ and $AuPb_3$) formed at the edges of the gold surfaces in the presence of 10 mM Tris-HCl solution (pH 8.0), and as observed in TEM image "b" in Figure 1B, the width of the Au NRs clearly increased to 13.2 ± 1.1 nm owing to the addition of Pb^{2+} to the solution. Therefore, the increased intensities of the SPR bands were caused by both the slight increase in the particle sizes and changes in the dielectric constant. Adding 3.0 mM $Na_2S_2O_3$ to the Au NR solution caused both TSPR and LSPR absorption to decrease slightly (Figure 1A curve "c"). This was observed because the $S_2O_3^{2-}$ could react with the Au NRs to form $Au(S_2O_3)_2^{3-}$ complexes that would both decrease SPR absorption and partly dissolve the Au NRs, which can be seen from TEM image "c" in Figure 1B (the Au NRs were 33.2 ± 3.5 nm long and 10.6 ± 1.1 nm wide). The LSPR absorption peak disappeared when 100 μM Pb^{2+} was added to the Au NRs in presence of $S_2O_3^{2-}$, and only a peak appeared at 530 nm. From TEM image "d" in Figure 1B, it was observed that the Au NRs had changed into spheres with diameters of 21.1 ± 4.4 nm, indicating that Pb^{2+} accelerated the etching effect in the $S_2O_3^{2-}$/Au NRs system. This phenomenon could be explained by $AuPb_2$ and $AuPb_3$ being formed on the gold surface in the presence of 10 mM Tris-HCl solution (pH 8.0) and 3 mM $Na_2S_2O_3$, resulting in a significant decrease in the electrode potential of the gold, and the increased dissolution rate that was observed.[28]

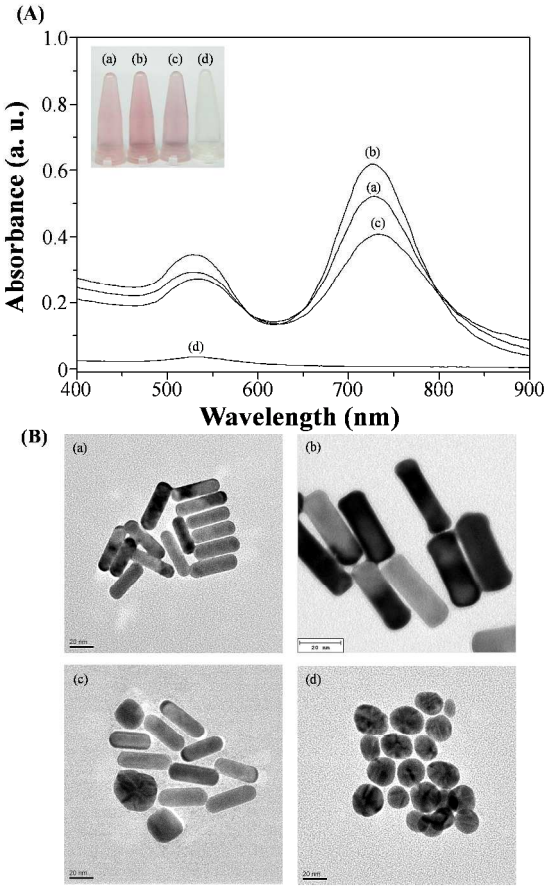

Figure 1. (A) UV–Vis absorbance spectra and (B) TEM images (scale bars = 20 nm) of Tris-acetate solutions (10 mM) of (a) the Au NRs and of the Au NRs in the presence of (b) Pb^{2+} ions (100 μM), (c) $S_2O_3^{2-}$ ions (3.0 mM), and (d) Pb^{2+} ions (100 μM) and $S_2O_3^{2-}$ ions (3.0 mM) at pH 8.0. The Au NR concentration was 51 pM. The absorbance is plotted in arbitrary units (a. u.). Inset: photographs of the Au NRs under the conditions mentioned above (a–d).

To further investigate the process involved in the leaching of the Au NRs, we used UV–Vis spectroscopy and TEM measurements to analyze Au NRs that had been left in 100 μM Pb^{2+} and 3 mM $Na_2S_2O_3$ in 10 mM Tris-HCl solution (pH 8.0) for different periods of time (1–15 min). We terminated the reactions at the specified times by adding a small amount of concentrated HCl, to bring the mixture to pH 3.0, which stopped the reaction effectively, as indicated by the fact that no changes in the UV spectra occurred for 12 h after this had been performed.[44] As is shown in Figure S1 (supplementary information), the Au NR solution became less intensely colored as the reaction time increased. Bone-like Au–Pb NRs were formed, as shown in Figure 1B image "b", suggesting that Au(0) and Pb(0) atoms were initially favor to be deposited on the {111} facets at each end of the Au NRs. This also suggests that the CTAB bilayers on the {110} surfaces of the Au NRs were not destroyed, and this would have mainly prevailed owing to the weak interactions between the negatively charged $Au(S_2O_3)_2^{3-}$ and positively charged CTA^+ ions. It is important to note that the position of the LSPR band shifted dramatically, from 750 to 680 nm, when the treatment time was increased

from 1 to 6 min (Figure S1). The large decreases and position changes in the LSPR peaks were mainly caused by changes in the shapes of the nanomaterials.

The abovementioned results imply that the Au NR leaching process had several steps, as shown in Figure S1. At less than 3.0 min of leaching in presence of $Na_2S_2O_3$, a redox reaction occurred at the solid–liquid interface, and $Au(S_2O_3)_2^{3-}$ complexes were formed on the surfaces of the Au NRs. Adding Pb^{2+} ions accelerated the leaching of the Au NRs. Pb^{2+} reacted with the gold to form Pb–Au alloys at each end of the Au NRs, resulting in a potential drop in the NRs' gold contents. The diameters of the Au NPs decreased from 25.9 ± 5.2 to 10.9 ± 2.3 nm between 12–15 min because the Au NPs were dissolved more as the reaction time increased. The morphological and size changes in Au NRs effectively proved the viability of using the system to measure Pb^{2+}.

Evidence for the Formation of $Au(S_2O_3)_2^{3-}$ Complexes and Pb–Au Alloys

We attempted to confirm that $Au(S_2O_3)_2^{3-}$ complexes were formed on the surfaces of the Au NRs by using IR, Raman, and dynamic light scattering techniques to analyze the Au NRs in presence of $S_2O_3^{2-}$ after a series of centrifugation and washing steps performed to ensure removing any unbound species. The IR and Raman spectra for the Au NRs in the presence of $Na_2S_2O_3$ (3.0 mM) are shown in Figures S2A and S2B, respectively. The $\nu_{(S-O)}$ and $\nu_{(S=O)}$ vibration modes for the $S_2O_3^{2-}$ adsorbed onto the Au NR surfaces were detected at 1000 and 1125 cm^{-1}, respectively, and these correspond to IR resonances. The $\nu_{(S-S)}$ and $\nu_{sym(S-O)}$ vibration modes were detected at 410 and 1030 cm^{-1}, respectively, and these correspond to Raman resonances.[45] A Zetasizer Nano ZS90 instrument was used to confirm that $S_2O_3^{2-}$ had been adsorbed onto the Au NR surfaces. The zeta potential of the Au NRs turned less positive as the $S_2O_3^{2-}$ concentration was increased, as observed in Figure S2C. These results further confirm that $S_2O_3^{2-}$ is likely to be present on the Au NR surfaces in the system.

Next, we used EDS, MALDI-MS, and XPS to prove that Pb–Au alloys formed on the Au NR surfaces, again performing a series of centrifugation and washing steps to ensure removing any unbound species. The EDS spectrum for the Au NPs in the presence of 100 μM Pb^{2+} and 3 mM $Na_2S_2O_3$ (see Figure S3) confirmed that Au and Pb atoms were present. The MALDI-MS spectra of the $S_2O_3^{2-}$/Au NRs in the absence and presence of Pb^{2+} are shown in Figure 2. Figure 2A illustrates the presence of cationic clusters $[Au_n]^+$ (n = 1−4) (m/z 196.967, 393.943, 590.920, and 787.900), indicating that the Au NRs were fragmented and vaporized during the analysis. The MS spectrum of $S_2O_3^{2-}$/Au NRs in the presence of Pb^{2+} is presented in Figure 2B, and the signals found at m/z 205.961, 402,936, 599.927, and 795.900 were assigned to $[Pb]^+$, $[AuPb]^+$, $[Au_2Pb]^+$, and $[Au_3Pb]^+$, respectively. The presence of Pb–Au alloys on the surfaces of Au NRs was also confirmed by the XPS data, using the alkyl chain C 1s binding energy (BE; 285 eV) as an internal reference. The BEs of the Au $4f_{7/2}$ electrons in the Au NRs were 84.3 eV in the absence of Pb^{2+} ions and 84.5 eV in the presence of Pb^{2+} ions, while the BEs of the $4f_{5/2}$ electrons in the Au NRs were 87.9 eV in the absence of Pb^{2+} ions and 88.3 eV in the presence of Pb^{2+} ions (Figure S4A). This implies that the reduction of Pb^{2+} ions caused the oxidation states of the Au NR surfaces to increase.[46, 47] The BEs of the Pb $4f_{7/2}$ and $4f_{5/2}$ electrons were 138.2 and 142.9 eV, respectively (Figure S4B), showing that Pb species were present. These results further confirmed that Pb–Au alloys formed on the surfaces of the Au NRs.

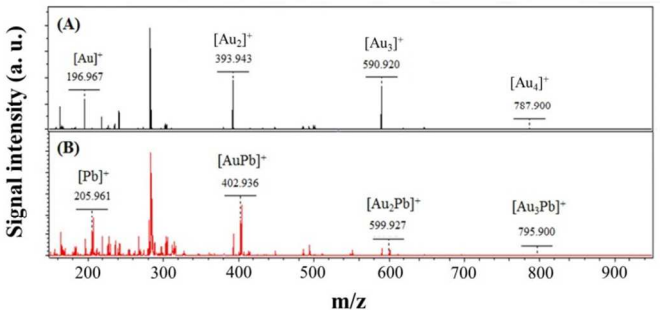

Figure 2. MS spectra of solutions containing 51 pM Au NRs and 3.0 mM $S_2O_3^{2-}$ in the absence (A) and presence (B) of Pb^{2+} ions (100 μM). A total of 500 pulsed laser shots were applied, with the laser fluence set at 51.25 μJ. The other conditions were the same as described in Figure 1.

Sensing mechanism

It is possible that $Au(S_2O_3)_2^{3-}$ complexes will form on the surfaces of the Au NRs, as observed from the mechanism shown in Scheme 1. $S_2O_3^{2-}$ ions can act as divalent-type soft ligands, forming stable complexes with low spin d^{10} Au^+ ions (log β $[Au(S_2O_3)_2^{3-}]$ = 26).[28] $S_2O_3^{2-}$ ions can also commonly act as monodentate ligands through the terminal sulfur atom, and this would allow them to establish strong σ bonds with gold ions that are stabilized by pπ–dπ back-bonding.[28] There are several studies to examine how foreign heavy metal ions affect the dissolution rate of gold in the thiosulfate and cyanide systems.[28-30] In the presence of $S_2O_3^{2-}$, adding Pb^{2+} to the system caused a monolayer of $AuPb_2$ and $AuPb_3$ alloys to form on the gold surfaces, causing the electrode potential of the gold to decrease and, in response, the dissolution rate to increase. This will lead to the color of the Au NR solution to gradually become less intense, and this phenomenon can be used to semi-quantify the Pb^{2+} in the aqueous solution. The Pb^{2+} concentrations can also be determined by monitoring changes in the SPR band ratio (which indicates the extent of the leaching effect), $(R_0 - R)/R_0$, of the Au NRs, where R and R_0 represent that SPR band ratio (A_{750}/A_{530}) of the Au NRs in the presence and absence of Pb^{2+} ions, respectively.

Optimization of the Assay

The effects of a number of factors, including the reagent concentration, the pH, the reaction temperature, and time, on the sensing system containing 1.0 μM Pb^{2+} were assessed to optimize the assay.

First, the effect of temperature on the leaching reaction was investigated over the range 25–80 °C. As is shown in Figure S5A, the leaching effect in the system increased with the increase in the reaction temperature, thus, reaching a maximum at 50 °C. The reason for this could be that the formation rate of $AuPb_2$ and $AuPb_3$ on the gold surface was enhanced at high reaction temperatures due to increasing the frequency of collisions between Pb^{2+} ions and Au NRs, resulting in an increased dissolution rate. However, reaction temperatures higher than 50 °C will have increased $S_2O_3^{2-}$ leaching rate on Au NR, decreasing the accelerated rate effect of Pb^{2+} ions on the leaching of the Au NRs. At 50 °C, the leaching effect in the system increased as time elapsed, reaching a maximum at 9 min, which was attributed to the leaching rate for the Au NRs reaching a maximum (Figure S1 inset). Therefore, a temperature of 50 °C and a reaction time of 10 min were chosen for subsequent tests.

Next, the effect of pH on the leaching reaction was investigated in the absence and presence of Pb^{2+}. As presented in Figure S5B, the effect of the pH was much more pronounced for solutions containing Pb^{2+} than for the solutions not containing Pb^{2+}. The maximum Au NR leaching rate was found at pH 8.0. In acidic media, $S_2O_3^{2-}$ ions will decompose to form sulfide, sulfate, sulfite, tetrathionate, trithionate, polythionates, and polysulfides.[28, 30] A higher pH may, therefore, improve the stability of $S_2O_3^{2-}$ ions and $S_2O_3^{2-}$/Au NRs. However, slightly lower Au NR leaching rates were found at pH values greater than 9.0, which could be attributed to passive layers of $Pb(OH)_2$, PbO, or $Au(OH)_3$ forming on the surfaces of the Au NRs at 50°C at such high pH values. A pH of 8.0 was used in subsequent experiments.

Finally, we determined the optimum Tris and $Na_2S_2O_3$ concentrations in the system. Figure S6 presents the different absorbance ratios and leaching effects that were found at different Tris and $Na_2S_2O_3$ concentrations in the absence and presence of Pb^{2+}. As observed from Figure S6A, the Tris concentration did not affect the leaching effects on the Au NRs. This was because Tris did not affect the stability of the Au NRs. Because of practical considerations, a Tris concentration of 10 mM was chosen for the subsequent experiments. Figure S6B shows that increasing the $Na_2S_2O_3$ concentration increased the leaching rate of the Au NRs in the presence of Pb^{2+}. However, the leaching rate reached a maximum at a $Na_2S_2O_3$ concentration of 3.0 mM, so the obtained concentration was used in subsequent experiments.

Selectivity and Sensitivity

We tested the selectivity of the $S_2O_3^{2-}$/Au NRs detection system toward Pb^{2+} ions using the optimized conditions by conducting experiments similar to those used to obtain Figure 1A "d", but replacing Pb^{2+} with another metal ion (K^+, Cd^{2+}, Ni^{2+}, Ca^{2+}, Hg^{2+}, Sr^{2+}, Cu^{2+}, Ba^{2+}, Fe^{2+}, Fe^{3+}, Ag^+, Na^+, Co^{2+}, or Mg^{2+}, each at a concentration of 100.0 μM). The leaching effects caused by 100.0 μM of the other metal ions were much smaller than that of 1.0 μM Pb^{2+} (Figure 3). We note that the Au NRs remained quite stable when $Na_2S_2O_3$ was absent, and the absorption spectra for the Au NRs were almost identical in the presence and absence 100.0 μM of these metal ions. Among the divalent metal ions, Cu^+/Cu^{2+} and Fe^{2+}/Fe^{3+} functioned as redox mediators that could increase the rate at which the Au NRs were leached by $S_2O_3^{2-}$ by decreasing the activation energy.[35, 48] Moreover, Cd^{2+}, Hg^{2+}, and Ag^+ ions partially reacted with the gold to form alloys on the gold surface, resulting in increased dissolution rates.[44, 49] In our experiments, Pb^{2+} ions seemed to react particularly well with the gold to form alloys, allowing the $S_2O_3^{2-}$/Au NRs probes to be highly specific toward Pb^{2+}. To further test the practicality of using the probe, we conducted measurements in mixtures containing 1.0 μM Pb^{2+} and various potentially interfering ions (K^+, Cd^{2+}, Ni^{2+}, Ca^{2+}, Hg^{2+}, Sr^{2+}, Cu^{2+}, Ba^{2+}, Fe^{2+}, Fe^{3+}, Ag^+, Na^+, Co^{2+}, and Mg^{2+}, each at a concentration of 100.0 μM). The results suggested that most of these metal ions did not interfere with the determination of Pb^{2+}. The presence of other metal ions caused the values for the leaching effect induced by Pb^{2+} to vary by below 0.04 units from the value for when only Pb^{2+} was present, in every case (Figure 3B).

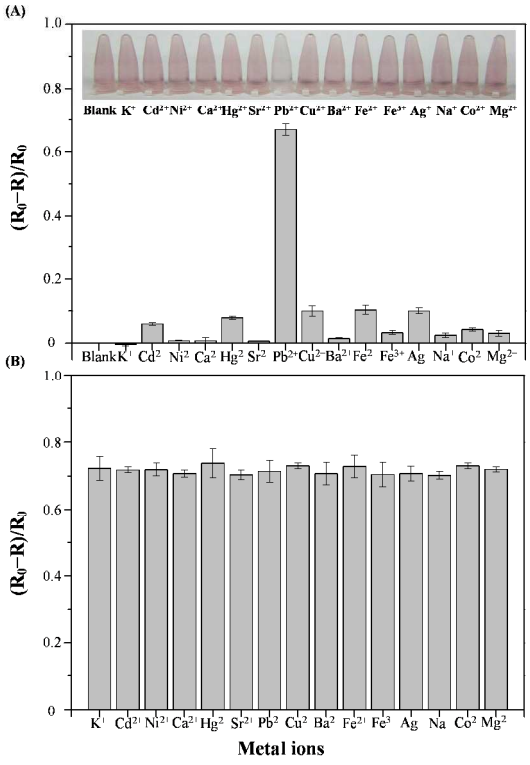

Figure 3. (A) Selectivity of the $S_2O_3^{2-}$/Au NRs probe toward Pb^{2+} ions (n = 3). The Pb^{2+} concentration was 1.0 μM, and the concentration of each of the other metal ions was 100 μM. Inset: photographs of the $S_2O_3^{2-}$/Au NRs probe in the presence of different metal ions. (B) Tolerance of the $S_2O_3^{2-}$/Au NRs probe in the presence of Pb^{2+} ions (n = 3). The Pb^{2+} concentration was 1.0 μM, and the concentration of each of the other metal ions was 100 μM.

We decided the sensitivity of the sensor by determining the lowest Pb^{2+} concentration detectable from the change in the color intensity of the Au NR solution. The intensity of the color

of the solutions decreased as the Pb^{2+} concentration was increased from 0 to 10 μM (Figure 4). The LOD for Pb^{2+} was 0.05 μM using the naked eye. The UV–Vis spectra of the Au NR solutions containing different Pb^{2+} concentrations, using the optimized conditions, were also recorded for use as a quantitative assay. Both TSPR and LSPR absorption clearly decreased with the increase in Pb^{2+} concentration, and these changes were owed to the Pb^{2+} ions accelerating the leaching of the Au NRs in the presence of $S_2O_3^{2-}$. A linear relationship was found between the leaching effect and the Pb^{2+} concentration over the range 10 nM–1.0 μM, and the linear correlation coefficient was 0.9969. The LOD for Pb^{2+}, defined as the concentration giving a signal-to-noise ratio of 3, was 4.3 nM using this technique suggesting that the probe is well suited for monitoring Pb^{2+} ions in samples of domestic and environmental water because the highest Pb^{2+} concentration permitted in drinking water by the US EPA is 75 nM.

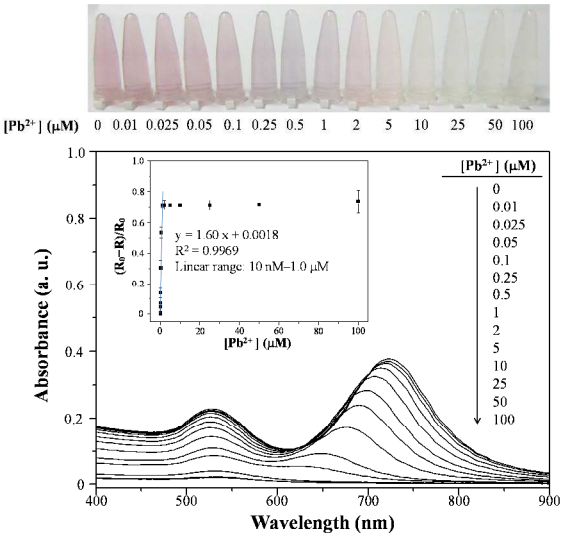

Figure 4. UV–Vis absorbance spectra and linear responses (inset) of the leaching effect plotted against the Pb^{2+} concentration (n = 3), and photographs of the $S_2O_3^{2-}$/Au NRs probe at different Pb^{2+} concentrations.

Application of the Assay

We expected that our $S_2O_3^{2-}$/Au NRs probes would have great potential for use analyzing Pb^{2+} in environmental water samples and biological samples. Pond and lake water samples from our campus, a seawater sample from the beach in Taichung city, and a urine sample from a healthy female were each filtered through a 0.2 μm membrane. The filtered samples were analyzed by AAS and found to be pure of Pb^{2+}, i.e., only the expected background concentrations were found. The trace Pb^{2+} concentrations in the pond, lake, seawater, and urine samples were all below the LOD of our method when 0.6 mL of a sample was added to 0.4 mL of 10 mM Tris-HCl solution containing $S_2O_3^{2-}$/Au NR probes. We demonstrated the feasibility of our approach to detecting Pb^{2+} ions in complicated matrices by using a standard addition method to determine the Pb^{2+} concentrations in the samples. There was a linear correlation between the $(R_0 - R)/R_0$ value and the spiked Pb^{2+} concentration in each sample, over the range 0.01–0.25 μM (Figure S7). The recoveries were 99.9%–108.1% (Table 1), and the LODs (for a signal-to-noise ratio of 3) for Pb^{2+} in these complex sample matrices were 5.3–9.7 nM. Our results suggest that this probe will be useful for detecting environmentally and biologically relevant Pb^{2+} concentrations.

The $S_2O_3^{2-}$/Au NRs probe, in conjunction with a standard addition method, was also used to determine the Pb^{2+} concentrations in a soil sample (Table 2), and the results of the assay were compared with measurements made using AAS. An F-test (the F value was 19 at the 95% confidence level) was performed, and the calculated F value for the soil sample at the 95% confidence level was 1.331, showing that there was no significant difference between the precisions of the new assay and the AAS method. A t-test (the t-test value was 2.776 at the 95% confidence level) was then performed, and the calculated t value for the soil sample at the 95% confidence level was 1.571, showing that the data obtained using the two methods were not significantly different. The new $S_2O_3^{2-}$/Au NRs probe can, therefore, be used to determine Pb^{2+} concentrations in real samples. This assay removes the need for complicated chemosensors to be synthesized or sophisticated equipment to be used.[50-53] In addition, compared to other non-DNA functionalized Au NP-based optical methods (Table 3), this novel $S_2O_3^{2-}$/Au NRs probe possesses several attractive features when compared with other reported methods: (1) facile and simplicity—expensive enzymes, DNA, and other recognition elements (gallic acid, glutathione, and azacrown ether), and sophisticated instruments (AAS, inductively coupled plasma mass spectrometry) are not required; (2) rapidity—it only takes 10 min to determine the Pb^{2+} concentration; (3) broad analytical range— the Pb^{2+} concentration was found over the range 10 nM – 1.0 μM with a linear coefficient of 0.9969. (4) sensitivity—the LOD for Pb^{2+} ions is 4.3 nM; (5) practicality—analysis of complicated samples (lake, pond, seawater, urine, and soil sample) is possible without performing tedious sample pretreatment.

Table 1: Parameters determined for the analysis of water samples and a urine sample spiked with Pb^{2+} using the proposed method.

Samples	Environmental water samples			Biological sample
	Pond	Lake	Seawater	Urine
Calibration equation	y = 1.72 x + 0.015	y = 1.73 x + 0.004	y = 1.63 x + 0.007	y = 1.61 x + 0.004
Correlation coefficient (R^2)	0.998	0.995	0.995	0.995
LOD (nM)	9.7	9.2	5.3	7.5
Recovery	99.9–104.7%	90.8–108.1%	96.2–103.9%	93.5–97.6%

The determinations were performed in triplicate.

Journal Name

RSCPublishing

ARTICLE

Table 2: Pb^{2+} concentrations found in a soil sample using the standard addition method.

Method	Soil sample
	Pb^{2+} concentration (ng/g)
Current assay	11.01 ± 0.13
AAS	11.19 ± 0.15

The determinations were performed in triplicate.

Table 3: Non-DNA functionalized Au NP-based colorimetric methods for the determination of Pb^{2+} ions.

Probe	Analytical range / LOD	Real samples	Ref.
Gallic acid-Au NPs	0.5 nM–1.0 μM / 0.25 nM	drinking water	19
Azacrown ether- Au NPs	–[a] / 0.1 mM	–[a]	20
Glutathione-Au NPs	0.1–50 μM / 100 nM	lake water	21
2-mercaptoethanol-Au NPs	50–500 nM / 45 nM	river water and Montana soil samples	22
Glutathione and pentapeptide (CALNN)-Au NPs	1–5 μM / 1 μM	HeLa cells	23
CALNN-Au NPs	0.1–30 μM / 0.1 μM	–[a]	24
Gallic acid-Au NPs	10–800 nM / 10 nM	drinking water	25
4-mercaptobutanol and $S_2O_3^{2-}$/Au NPs	0.5–10 nM / 0.2 nM	Montana soil and urine samples	26
Glycine-Au NPs	2–30 μM / 5 μM	–[a]	27
Au NPs/ $S_2O_3^{2-}$ and 2-mercaptoethanol	2.5 nM–10 μM /0.5 nM	Montana soil and river samples	28
BSA-Au NPs/ $S_2O_3^{2-}$ and 2-mercaptoethanol	10 nM–1.0 μM / 5 nM	seawater, urine and blood samples	29
$S_2O_3^{2-}$/Au NPs	1–6 μM / 40 nM	drinking water	30
$S_2O_3^{2-}$/Au NRs	10 nM–1.0 μM / 4.3 nM	pond, lake, seawater, urine and soil samples	This study

a: not provided

Conclusions

We have developed a colorimetric probe based on $S_2O_3^{2-}$/Au NRs for the selective detection of Pb^{2+} ions. The formation of Pb–Au alloys on the surfaces of Au NRs plays an important role in the assay, determining the sensitivity and selectivity of the method. This conclusion was supported by TEM, EDS, MALDI-MS, and absorption analyses. The probe is sensitive toward Pb^{2+} (LOD = 4.3 nM), and has a high degree of selectivity for Pb^{2+} over most potentially interfering metal ions in aqueous solutions. These results allow us to foresee great potential for using Au NRs of various shapes because of their outstanding optical properties, including strong and sharp longitudinal SPR absorption bands in the visible and near-infrared regions. The bioconjugation of Au NRs is essential to allow excellent sensitivities, selectivities, and throughput rates to be achieved. In the future, we will focus on preparing different bioconjugated Au NRs, which we hope could be used for the simultaneous analysis of several analytes of interest, such as metal ions and proteins.

Acknowledgements

This study was supported by the National Science Council of Taiwan under contract NSC 101-2113-M-018-001-MY2 and the Ministry of Science and Technology under contract MOST 103-2120-S-018 -007. The authors would like to thank Enago (www.enago.tw) for correcting the English language in this manuscript.

Notes and references

Department of Chemistry, National Changhua University of Education,1, Jin-De Road, Changhua City, Taiwan; Tel: 011-886-4-7232105-3522
E-mail: linywjerry@cc.ncue.edu.tw

Electronic Supplementary Information (ESI) available: [Figure S1. Photograph, UV–Vis absorption spectra, and TEM images of the Au NRs after different amounts of time in the presence of 100 μM Pb^{2+} and 3.0 mM $S_2O_3^{2-}$ at 50 °C. Figure S2. (A) FT-IR spectrum, (B) Raman spectrum, and (C) Zeta potential of the Au NRs in the presence of different concentrations of $S_2O_3^{2-}$. Figure S3. EDS spectrum of the Au NRs in the presence of 3.0 mM $S_2O_3^{2-}$ and 100 μM Pb^{2+} at 50 °C. Figure S4. (A) Binding energies of the $4f_{7/2}$ and $4f_{5/2}$ electrons of the $S_2O_3^{2-}$/Au NRs in the absence (black line) and presence (red line) of Pb^{2+} ions. (B) Relative XPS intensity plotted against the binding energy, with the peaks for the Pb $4f_{7/2}$ and $4f_{5/2}$ electrons marked. Figure S5. Absorbance ratios and leaching effects for the $S_2O_3^{2-}$/Au NRs in the absence and presence of Pb^{2+}, using a Tris-HCl buffer solution (10 mM), at different (A) temperatures and (B) pH values. Figure S6. Absorbance ratios and leaching effects for the Au NRs in the absence and presence of Pb^{2+} at different concentrations of (A) Tris-HCl buffer and (B) $Na_2S_2O_3$. Figure S7. Standard addition analyses of (A) pond water, (B) lake water, (C) seawater, and (D) urine samples using the $S_2O_3^{2-}$/Au NRs probe.]. See DOI: 10.1039/b000000x/

1. M. Meadows-Oliver, *J. Pediatr. Health Care*, 2012, **26**, 213-215.

2. M. P. Iqbal, *Pak. J. Pharm. Sci.*, 2012, **25**, 289-294.
3. C. Sobin, N. Parisi, T. Schaub, M. Gutierrez and A. X. Ortega, *Arch. Environ. Con. Tox.*, 2011, **61**, 521-529.
4. J. A. Menezes, G. F. D. Viana and C. R. Paes, *Environ. Monit. Assess.*, 2012, **184**, 2593-2603.
5. A. N. Shipway, E. Katz and I. Willner, *ChemPhysChem*, 2000, **1**, 18-52.
6. S. G. Penn, L. He and M. J. Natan, *Curr. Opin. Chem. Biol.*, 2003, **7**, 609-615.
7. E. Roduner, *Chem. Soc. Rev.*, 2006, **35**, 583-592.
8. Y. W. Lin, C. C. Huang and H. T. Chang, *Analyst*, 2011, **136**, 863-871.
9. S. Eustis and M. A. El-Sayed, *Chem. Soc. Rev.*, 2006, **35**, 209-217.
10. D. Pissuwan, S. M. Valenzuela and M. B. Cortie, *Trends Biotechnol.*, 2006, **24**, 62-67.
11. M. Hu, J. Chen, Z.-Y. Li, L. Au, G. V. Hartland, X. Li, M. Marquez and Y. Xia, *Chem. Soc. Rev.*, 2006, **35**, 1084-1094.
12. A. Moores and F. Goettmann, *New J. Chem.*, 2006, **30**, 1121-1132.
13. H. Xu, B. X. Liu and Y. Chen, *Microchim. Acta*, 2012, **177**, 89-94.
14. M. R. Knecht and M. Sethi, *Anal. Bioanal. Chem.*, 2009, **394**, 33-46.
15. Y. W. Lin, C. W. Liu and H. T. Chang, *Anal. Methods-Uk*, 2009, **1**, 14-24.
16. Z. D. Wang, J. H. Lee and Y. Lu, *Adv. Mater.*, 2008, **20**, 3263-3267.
17. H. Wei, B. L. Li, J. Li, S. J. Dong and E. K. Wang, *Nanotechnology*, 2008, **19**, 095501-095505.
18. K. Yoosaf, B. I. Ipe, C. H. Suresh and K. G. Thomas, *J. Phys. Chem. C*, 2007, **111**, 12839-12847.
19. N. Ding, Q. A. Cao, H. Zhao, Y. M. Yang, L. X. Zeng, Y. J. He, K. X. Xiang and G. W. Wang, *Sensors*, 2010, **10**, 11144-11155.
20. A. Alizadeh, M. M. Khodaei, C. Karami, M. S. Workentin, M. Shamsipur and M. Sadeghi, *Nanotechnology*, 2010, **21**, 315503-315510.
21. F. Chai, C. A. Wang, T. T. Wang, L. Li and Z. M. Su, *ACS Appl. Mater. Interfaces*, 2010, **2**, 1466-1470.
22. Y. L. Hung, T. M. Hsiung, Y. Y. Chen, Y. F. Huang and C. C. Huang, *J. Phys. Chem. C*, 2010, **114**, 16329-16334.
23. D. R. Zhu, X. K. Li, X. Liu, J. N. Wang and Z. X. Wang, *Biosens. Bioelectron.*, 2012, **31**, 505-509.
24. X. K. Li and Z. X. Wang, *Chem. Res. Chin. Univ.*, 2010, **26**, 194-197.
25. K. W. Huang, C. J. Yu and W. L. Tseng, *Biosens. Bioelectron.*, 2010, **25**, 984-989.
26. Y. L. Hung, T. M. Hsiung, Y. Y. Chen and C. C. Huang, *Talanta*, 2010, **82**, 516-522.
27. K. Hamaguchi, H. Kawasaki and R. Arakawa, *Colloid Surf. A-Physicochem. Eng. Asp.*, 2010, **367**, 167-173.
28. Y. Y. Chen, H. T. Chang, Y. C. Shiang, Y. L. Hung, C. K. Chiang and C. C. Huang, *Anal. Chem.*, 2009, **81**, 9433-9439.
29. Y. F. Lee and C. C. Huang, *ACS Appl. Mater. Interfaces*, 2011, **3**, 2747-2754.
30. Y. J. Zhang, Y. M. Leng, L. J. Miao, J. W. Xin and A. G. Wu, *Dalton Trans.*, 2013, **42**, 5485-5490.
31. C. Sönnichsen, T. Franzl, T. Wilk, G. von Plessen, J. Feldmann, O. Wilson and P. Mulvaney, *Phys. Rev. Lett.*, 2002, **88**, 0774021-0774024.
32. S. Link, M. B. Mohamed and M. A. El-Sayed, *J. Phys. Chem. B*, 1999, **103**, 3073-3077.
33. S. Link and M. A. El-Sayed, *J. Phys. Chem. B*, 2005, **109**, 10531-10532.
34. C. Yu and J. Irudayaraj, *Anal. Chem.*, 2007, **79**, 572-579.
35. T. Wen, H. Zhang, X. P. Tang, W. G. Chu, W. Q. Liu, Y. L. Ji, Z. J. Hu, S. Hou, X. N. Hu and X. C. Wu, *J. Phys. Chem. C*, 2013, **117**, 25769-25777.
36. X. Liu, S. Y. Zhang, P. L. Tan, J. Zhou, Y. Huang, Z. Nie and S. Z. Yao, *Chem. Commun.*, 2013, **49**, 1856-1858.
37. J. M. Liu, L. Jiao, M. L. Cui, L. P. Lin, X. X. Wang, Z. Y. Zheng, L. H. Zhang and S. L. Jiang, *Sens. Actuator B-Chem.*, 2013, **188**, 644-650.
38. P. K. Jain, S. Eustis and M. A. El-Sayed, *J. Phys. Chem. B*, 2006, **110**, 18243-18253.
39. B. Pan, L. Ao, F. Gao, H. Tian, R. He and D. Cui, *Nanotechnology*, 2005, **16**, 1776-1780.
40. P. K. Sudeep, S. T. S. Joseph and K. G. Thomas, *J. Am. Chem. Soc.*, 2005, **127**, 6516-6517.
41. M. Rex, F. E. Hernandez and A. D. Campiglia, *Anal. Chem.*, 2006, **78**, 445-451.
42. C.-D. Chen, S.-F. Cheng, L.-K. Chau and C. R. C. Wang, *Biosens. Bioelectron.*, 2007, **22**, 926-932.
43. B. Nikoobakht and M. A. El-Sayed, *Chem. Mater.*, 2003, **15**, 1957-1962.
44. Y. F. Huang, Y. W. Lin and H. T. Chang, *Nanotechnology*, 2006, **17**, 4885-4894.
45. M. I. Jeffrey, K. Watling, G. A. Hope and R. Woods, *Miner. Eng.*, 2008, **21**, 443-452.
46. Y. S. Wu, F. F. Huang and Y. W. Lin, *ACS Appl. Mater. Interfaces*, 2013, **5**, 1503-1509.
47. C. I. Wang, C. C. Huang, Y. W. Lin, W. T. Chen and H. T. Chang, *Anal. Chim. Acta*, 2012, **745**, 124-130.
48. X. Guo, Q. Zhang, Y. H. Sun, Q. Zhao and J. Yang, *Acs Nano*, 2012, **6**, 1165-1175.
49. Z. S. Yang, Y. W. Lin, W. L. Tseng and H. T. Chang, *J. Mater. Chem.*, 2005, **15**, 2450-2454.
50. H. N. Kim, W. X. Ren, J. S. Kim and J. Yoon, *Chem. Soc. Rev.*, 2012, **41**, 3210-3244.
51. F. LLerena, M. Maynar, G. Barrientos, R. Palomo, M. C. Robles and M. J. Caballero, *Eur. J. Appl. Physiol.*, 2012, **112**, 3027-3031.
52. P. C. Kruger, M. S. Bloom, J. G. Arnason, C. D. Palmer, V. Y. Fujimoto and P. J. Parsons, *J. Anal. At. Spectrom.*, 2012, **27**, 1245-1253.
53. I. S. Trujillo, E. V. Alonso, A. G. de Torres and J. M. C. Pavon, *Microchem J.*, 2012, **101**, 87-94.